Deep UV photon-counting detectors and applications

Deep UV Photon-Counting Detectors and Applications

Gary A. Shaw†, Andrew M. Siegel, Joshua Model, Adam Geboff
MIT Lincoln Laboratory, Lexington, MA 02420-9185
Stanislav Soloviev, Alexey Vert, Peter Sandvik
GE Global Research, 1 Research Circle, Niskayuna, NY 12309

ABSTRACT

Photon counting detectors are used in many diverse applications and are well-suited to situations in which a weak signal is present in a relatively benign background. Examples of successful system applications of photon-counting detectors include ladar, bio-aerosol detection, communication, and low-light imaging. A variety of practical photon-counting detectors have been developed employing materials and technologies that cover the waveband from deep ultraviolet (UV) to the near-infrared. However, until recently, photoemissive detectors (photomultiplier tubes (PMTs) and their variants) were the only viable technology for photon-counting in the deep UV region of the spectrum. While PMTs exhibit extremely low dark count rates and large active area, they have other characteristics which make them unsuitable for certain applications. The characteristics and performance limitations of PMTs that prevent their use in some applications include bandwidth limitations, high bias voltages, sensitivity to magnetic fields, low quantum efficiency, large volume and high cost.

Recently, DARPA has initiated a program called Deep UV Avalanche Photodiode (DUVAP) to develop semiconductor alternatives to PMTs for use in the deep UV. The higher quantum efficiency of Geiger-mode avalanche photodiode (GM-APD) detectors and the ability to fabricate arrays of individually-addressable detectors will open up new applications in the deep UV. In this paper, we discuss the system design trades that must be considered in order to successfully replace low-dark count, large-area PMTs with high-dark count, small-area GM-APD detectors. We also discuss applications that will be enabled by the successful development of deep UV GM-APD arrays, and we present preliminary performance data for recently fabricated silicon carbide GM-APD arrays.

1. INTRODUCTION

At an ultraviolet wavelength of 250nm, a source with just 1mW of optical output power produces over 1,000,000 billion (10^{15}) photons per second. While this number seems unfathomably large, there are in fact many applications in which detecting and time-tagging the arrival of individual photons is desirable. The ultraviolet (UV) region of the electromagnetic spectrum refers to light with wavelengths ranging from about 10nm up to 400nm. The UV spectrum is further subdivided into regions or subbands, some of them overlapping, as summarized in Table 1. In the literature, the boundaries of these regions are not consistently defined, and other names may be used to refer to the subbands. For example, the term "deep-UV" is often used to refer to the UV-C band.

Table 1: *Ultraviolet spectral region and subband definitions*

Name of Ultraviolet Subband	Band Abbreviation	Wavelength Range (nm)	Photon Energy (eV)
Ultraviolet A, long wave, or black light	UVA	400 –320	3.10–3.94
Near	NUV	400 – 300	3.10–4.13
Ultraviolet B or medium wave	UVB	320 –280	3.94–4.43
Middle	MUV	300 –200	4.13–6.20
Ultraviolet C, short wave, or germicidal	UVC	280 – 100	4.43–12.4
Far	FUV	200 – 122	6.20–10.2
Vacuum	VUV	200 – 10	6.20–124
Extreme	EUV	121 – 10	10.2–124

†Communication: shaw@ll.mit.edu, MIT Lincoln Laboratory, 244 Wood Street, Lexington, MA 02420-9185

Advanced Photon Counting Techniques III, edited by Mark A. Itzler, Joe C. Campbell,
Proc. of SPIE Vol. 7320, 73200J · © 2009 SPIE · CCC code: 0277-786X/09/$18 · doi: 10.1117/12.820825

There are a number of diverse reasons for interest in deep-UV photon-counting detectors. One advantage to optical systems that operate at short wavelengths is that finer diffraction-limited resolution that can be achieved for a given size aperture. Another advantage is the absence of solar background in the deep-UV spectral band. At wavelengths from about 280 down to 200nm, termed the solar-blind region of the UV spectrum, ozone and oxygen in the atmosphere absorb all of the UV radiation from the sun, resulting in benign backgrounds even in full mid-day sun. However, in order to take advantage of the low backgrounds in this region, the detector must either be totally unresponsive to light from the near-UV and visible portion of the solar spectrum (solar-blind), or the near-UV and visible background flux must be suppressed by appropriately designed filters. In practice, it is difficult to design and fabricate UV detectors that are totally unresponsive to longer wavelength background in the near-UV and visible, so an appropriately designed filter is generally required, even with so-called "solar-blind" detectors.

The same phenomena that are responsible for the existence of benign backgrounds, namely strong absorption and scattering of UV-C solar illumination by the atmosphere, are also an impediment to applications requiring active illumination such as stand-off ladar.

2. PHOTON COUNTING DETECTORS

A variety of device technologies have been employed to realize photon-counting detectors. Not all technologies function in the deep-UV and of those that do, there are significant performance issues to consider when selecting a detector technology for a particular application. In this section, system-level performance metrics applicable to photon-counting detector technology are identified and then employed as the basis for comparing performance of both commercial off-the-shelf (COTS) and emerging research-grade detectors.

2.1. System-Level Detector Performance Metrics

In considering the various detector technologies that might be employed in a particular deep-UV photon-counting application, the performance measures most frequently of interest include the efficiency of the detector in converting photons to detectable current pulses, the internally-generated false count ("dark count") rate, and the maximum useable counting rate, or bandwidth, of the detector. A parameter related to detection bandwidth is the temporal stability with which the arrival of a photon can be measured, called "timing jitter". Depending upon detector specifics, the photon conversion efficiency may be quoted either as quantum efficiency (QE) or as single photon detection efficiency (SPDE). The mechanisms responsible for the generation of dark counts also vary with the detector technology and design. As a rule of thumb, the dark count rate grows in proportion to the active area of the detector, so comparisons of dark count rate performance across detectors should always be normalized by the active area of the detector.

For the reasons discussed in Section 1, the responsivity or QE of the detector at longer wavelengths (out-of-band) may be an important factor in determining the utility of a particular detector technology for deep-UV, especially when the application involves solar backgrounds.

Even when the performance metrics mentioned thus far are suitable for an intended application, pragmatic considerations of size, weight, power consumption, sensitivity to environmental extremes, and cost may eliminate a particular detector technology from consideration.

2.2. Commercial Detector Technology

The two broad classes of photon-counting detectors addressed in this paper are PMTs and Geiger-mode APDs (GM-APDs). Within each of these classes, design and material variations lead to families of devices with wavelength-dependent performance differences. For simplicity, we identify a single commercial device within each class as a baseline against which to compare the performance of emerging wide-band gap GM-APD devices. There is no implied endorsement in our particular selection of representative commercial detectors.

2.2.1. Photomultiplier tubes

Channel photomultipliers (CPM) are a specific class of PMT that exhibit a low dark count density, good discrimination performance, and commercial availability. The Perkin Elmer MP-1921 channel photomultiplier module[1] (CPM) includes an internal high-voltage bias supply and discrimination circuit that delivers a digital pulse for each photon detected. The MP-1921 has a large active area (1.9cm^2), and an extremely low dark count rate (<10 cps). Furthermore, the CPM employs a cesium telluride (CsTe) photoemissive cathode resulting in a high degree of solar rejection, since the quantum efficiency rolls off steeply at around 300nm. Photos of the CPM and an associated quantum efficiency curve are shown in Figure 1. The 16mm CPM head for the module, shown in Figure 1c, only consumes about 45mm^3 of the total packaged module volume. The remaining 280mm^3 are devoted to the high-voltage bias supply, discriminator circuitry and RS-232 interface.

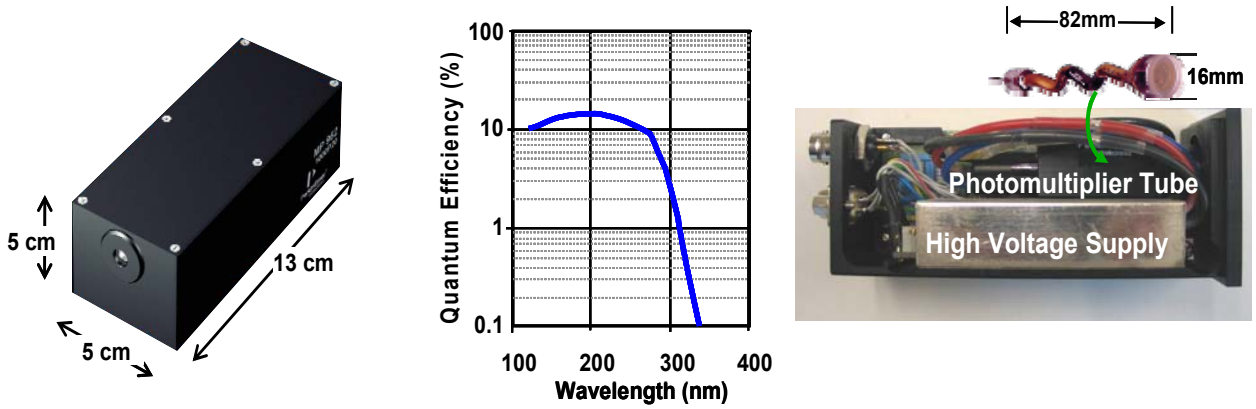

(a) (b) (c)

Figure 1: *(a) Perkin Elmer channel MP-series photomultiplier module (b) quantum efficiency as a function of wavelength (c) interior view of module showing high-voltage power supply, photomultiplier tube, and interface wiring.*

2.2.2. Geiger-mode APDs

Silicon GM-APDs are relatively mature. When operated in Geiger-mode to count individual photon arrivals, the avalanche current must be quenched, either actively or passively, prior to re-arming the APD. Three increasingly more complicated quenching schemes are illustrated in Figure 2.

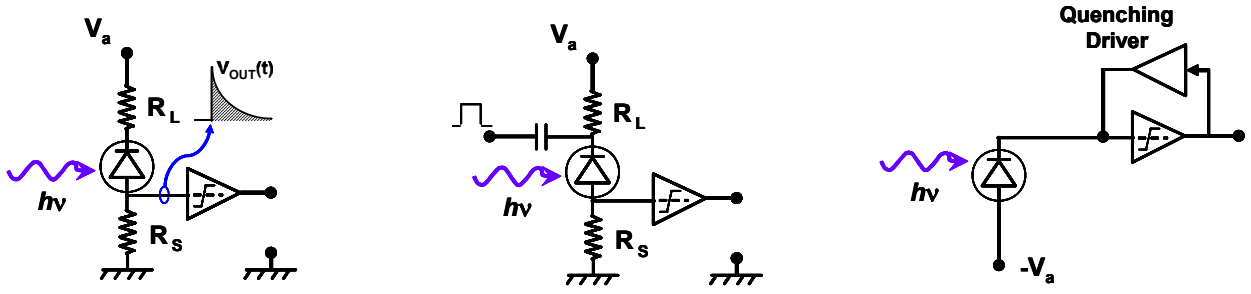

(a) (b) (c)

Figure 2: *Three GM-APD quenching schemes (a) asynchronous passive quenching, with reset time dominated by the R_LC_J time constant. (b) Gated quenching, with an enable pulse prebiasing the APD prior to an event of interest. (c) asynchronous active quenching, with the reset time determined by the quenching driver design.*

During the time between firing of the APD and resetting, the APD is essentially blind to the arrival of additional photons. This dead time can be modeled as an average loss in sensitivity, referred to as a blocking loss. The speed with which the re-arming operation can occur is determined by the RC time constant of the bias circuit in passive quenching mode, or by the design of the quenching circuit in active-quenching mode. In order to achieve fast recovery of the GM-APD, low capacitance, and thus small active areas are desirable. As the active area of the APD increases, the capacitance and dark count rate tend to grow in proportion.

2.2.3. Pixellated Geiger-mode APD

Pixellated GM-APD arrays, consisting of many individual passively quenched APDs connected in parallel, were designed to overcome the high blocking loss of a single large-area GM-APD detector. Silicon pixellated GM-APDs are commercially available from several sources[2]-[3]. For the purpose of photon-counting in the deep-UV, not all Si GM-APD device designs are equally effective. UV-C single photon energy levels are significantly higher than the band-gap of silicon (> 4.5eV versus 1.12 eV) so photon absorption tends to occur near the surface of the APD. Consequently, APD designs can be optimized for better performance in the UV-C band. Hamamatsu Corporation has a family of Si GM-APD arrays with SPDEs comparable to or better than the QE of CsTe PMTs in the UV-C band. Figure 3 shows a Hamamatsu 1mm x 1mm Multi-Pixel Photon Counter (MPPC) along with an illustration of the method of parallel connection of the individual APDs employed in the MPPC device.

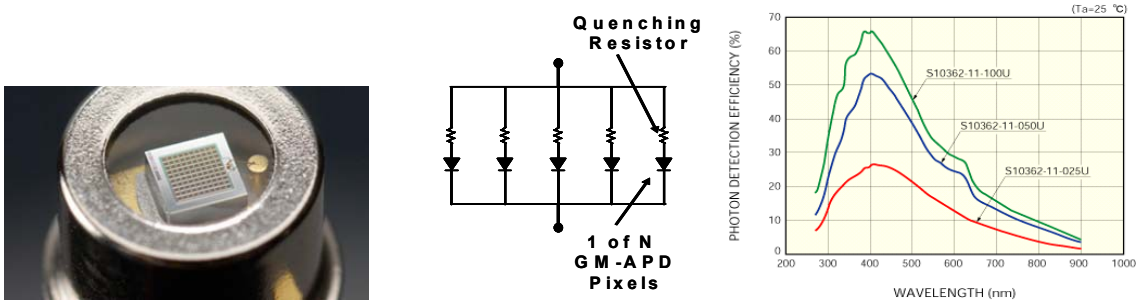

(a) (b) (c)

Figure 3: *Hamamatsu Multiple Pixel Photon Counting (MPPC) array (a) 50μm pixel detector (b) parallel connection of individual GM-APD detectors comprising the array (c) manufacture's nominal PDE as a function of pixel sizes.*

The MPPC device is available with 3 different pixel sizes (25μm, 50 μm, 100 μm) and three different physical sizes (1mmx1mm, 2mmx2mm, 3mmx3mm). As shown in Table 2, for the 1mmx1mm part, the choice of pixel size primarily affects the SPDE (in part due to fill factor), the aggregate array dark count, and the recovery time (which limits the maximum achievable bandwidth).

Table 2: *Hamamatsu specifications for passively-quenched MPPC GM-APD arrays*

Parameter	Hamamatsu S10362-11 Series Device Suffix			Units
	-025C	-050C	-100C	
Physical area	1x1	1x1	1x1	mm
Number pixels	40x40	20x20	10x10	
Pixel size	25	50	100	μm
Fill factor	30.8	61.5	78.5	%
SPDE at 400nm	25	50	65	%
SPDE at 270nm	8	12	20	%
Dark count rate	300	400	600	kHz
Recovery time	20	50	100	ns

While photon-counting in the deep-UV can be accomplished with silicon GM-APDs, the fact that silicon responsivity peaks in the visible, as shown in Figure 3c, means that effective blocking filters for suppression of out-of-band (e.g. near-UV and visible) flux are difficult to design and fabricate.

All of the pixels in commercial pixellated GM-APDs are connected in parallel. This parallel connection architecture results in a sequence of charge pulses that, over the linear region of the APD (i.e., small signal, low blocking loss regime,) is proportional to the number of simultaneous photon detections at any instant. However, the fact that the APDs are not individually addressable or controllable precludes use of MPPC arrays for imaging applications.

3. SOLAR-BLIND GEIGER-MODE AVALANCHE PHOTODIODE DETECTOR ARRAYS

As indicated in the previous section, CsTe photomultiplier tubes are solar-blind detectors suitable for many deep-UV sensing applications with large active area, low dark count,. However, the bandwidth of PMTs is too low for some applications, and their size and cost precludes the development of arrays for small form-factor imaging applications.

Commercially available Si APDs demonstrate moderate quantum efficiencies in the ultraviolet and solar-blind range, but require expensive optical filters to achieve a high solar photon rejection ratio with wide field of view as their response extends through the visible wavelength range. Si-based APDs with very low dark counts were demonstrated when they were cooled to liquid nitrogen temperatures[4]. However, typical dark current densities of these devices at a gain of more than 10 are on the order of ~100 nA/cm^2 at room temperature, which makes them hard to operate in a single-photon detection mode without cooling. In addition, the electronic properties of silicon impose an upper limit on the operating temperature of silicon-based electronic devices at roughly 200 °C for devices fabricated on conventional bulk silicon substrates due to rapidly increasing leakage current.

While Si detectors and PMTs are often detectors of choice, novel GaN-based detectors have seen advancements recently. GaN-based APDs were demonstrated with a high sensitivity in the solar-blind region and gain of more than 1000[5]-[7]. Reported dark currents at a gain of 1000 were typically more than 100 nA/cm^2 for these devices, likely due to high defect densities present in the GaN material.

SiC-based APDs have been demonstrated with high quantum efficiencies in the solar-blind wavelength range, and have been shown to have high gain and low dark currents[8]-[12]. Recently reported devices with dark current densities of 63 nA/cm^2 demonstrated a gain of more than 10,000 and also showed a very low noise equivalent power of 20 fW[13].

Typical SiC-based photo detectors show response in the range from 200 to 400 nm with a peak value between 270 and 300 nm. For solar-blind applications, in order to limit the SiC APD response to the solar-blind wavelengths, an optical filter may be used to reject the light above approximately 280 nm, where some light absorption occurs due to indirect nature of SiC band structure.

3.1. Silicon Carbide GM-APD Array Development

APD epitaxial structures with separate absorption and multiplication (SAM) regions were designed and optimized. Typical SAM-APDs are designed to achieve reach-through (when an electric field in the absorption layer reaches N+ cap layer) prior to reaching high gain in order to obtain fast response. This enhances the likelihood that photogenerated carriers in the absorption region will be swept into the multiplication region and contribute to photocurrent. However, the appreciable electric field in the absorption region increases the overall dark current and thereby decreases the signal-to-noise ratio of the detector. The 4H-SiC SAM-APDs presented here were intentionally designed to operate under non-reach-through conditions.

A schematic cross-sectional view of the 4H-SiC SAM-APD is shown in Figure 4, while the 2-D distribution of electric field at an avalanche breakdown voltage simulated with SILVACO model is shown in Figure 5. Note, that maximum electric field is uniformly distributed in a bulk of the device (not at the edges) due to a positive bevel structure. Using n-type doped materials for the absorption and charge layer was beneficial as the diffusion length of minority holes in n-type 4H-SiC is significantly longer than that of minority electrons in p-type. This results in the diffusion of

comparatively more carriers into the avalanche region which give rise to higher photocurrents particularly at higher energies where the photon penetration depth is small.

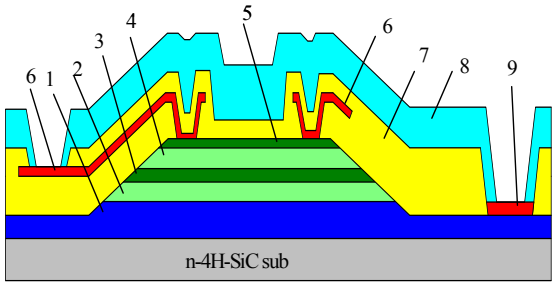

Figure 4: *Schematic cross-sectional view of the 4H-SiC SAM-APD , 1 – p-layer, 2 – n^--layer, 3 – n^- layer, 4 – n^--layer, 5 – n^+-layer, 6 – n-contact, 7 – SiO_2, 8 – filter, 9 – p-contact*

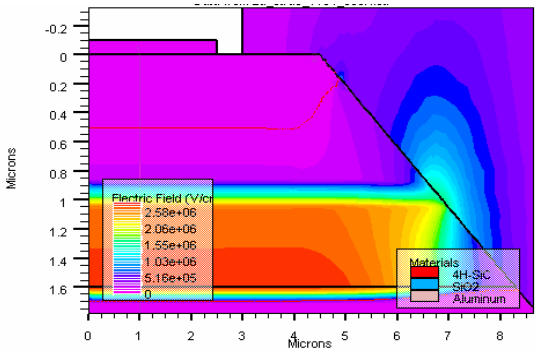

Figure 5: *2-D distribution of electric filed at an avalanche breakdown voltage*

3.2. Fabrication of SiC APD arrays

SiC APD arrays, as well as single APD devices, were fabricated using 3-inch diameter n-doped 4H-SiC substrates purchased from Cree Research (Durham, NC). The array APD devices had effective p-n junction diameters of 100 µm and with areas of UV light exposure of 44 µm in diameter. Single APD test devices varied from 200 to 500 µm. The APD structure consisted of a 0.2 µm n^+ cap layer (N_d=2x10^{18} cm^{-3}), a 0.6 µm n^--layer (N_d=2.0x10^{16} cm^{-3}), a 0.15 µm n^--layer (N_d=6x10^{17} cm^{-3}), a 0.6 µm n^--layer (N_d=1.4x10^{16} cm^{-3}), and a 2 µm p^+-layer (N_A=10^{18} cm^{-3}).

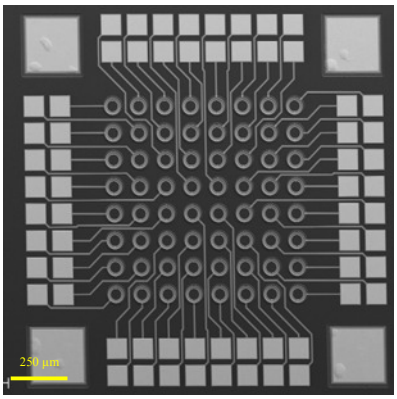

(a)

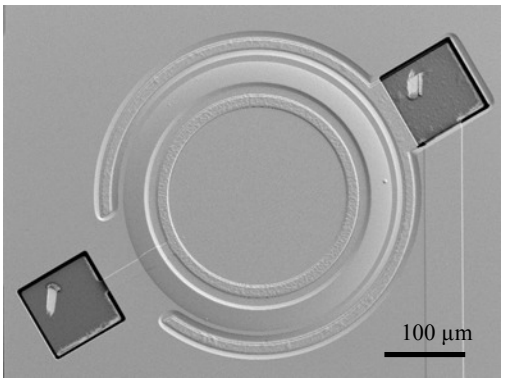

(b)

Figure 6: *SEM images of (a) SiC APD array and (b) single test APD device with an optical filter.*

The processing steps used to fabricate the devices included mesa etching, passivation deposition, cathode and anode contact formation, and passivation removal in the active area. Reactive ion etching was used to define the mesas with the beveled geometry in order to eliminate edge breakdown effects. A thermally grown SiO_2 film was deposited to passivate the surface. Ni was sputtered to form the n-type contacts and a multiple-layer stack of Ti/Al/Ti/Ni was deposited to form the p-type contacts. Both contacts were annealed simultaneously at 1050ºC in a N_2 ambient. Finally, Ti/Au metal pads were deposited on top of the ohmic contacts and the passivation layer was removed in the active region by wet etching. In order to limit the response of SiC APDs to the solar-blind wavelengths, an optical filter was used to reject the light at wavelengths above 280 nm. A thin film optical filter comprised of HfO_2 and SiO_2 layers was used to provide both a packaged version and a version with the filter deposited directly on the SiC detector. The optical filter deposition was performed by Barr Associates Inc.[14] Inductively coupled plasma etching was used to open contact windows in the filter after its deposition on APD devices. Figure 6 shows SEM images of (a) SiC APD array and (b) single test APD device with an optical filter.

3.3. SiC APD performance

A typical dark current and gain characteristics for a group of devices from the best fabricated APDs are shown in Figure 7, while Figure 8 shows the spectral response of unfiltered 4H-SiC APDs measured at two different bias voltages in the wavelengths range from 200 to 400 nm.

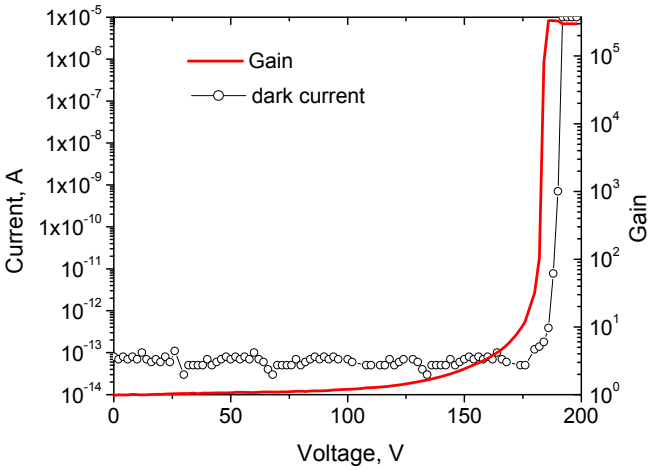

Figure 7: *Dark current and gain characteristics of SiC APD.*

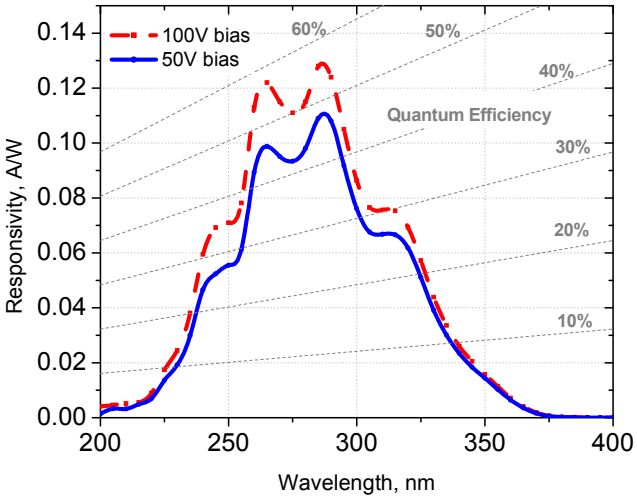

Figure 8: *Spectral response of unfiltered 4H-SiC APDs measured at two different bias voltages in the wavelength range from 200 to 400 nm.*

The responsivity and external quantum efficiency measured at a reverse bias of 50 V are considered to be representative for the linear regime without any gain. At unity gain, the external quantum efficiency was 47% at 280 nm. With the bias increased to 100 V, the responsivity increase was likely caused by a slight increase in the external quantum efficiency as a result of modulation of the depletion width and an increase of the gain. Those two effects are very difficult to separate, but the external quantum efficiency did not exceed 57% at 280 nm. Several noticeable characteristic features affecting smoothness of the responsivity are attributed to the oxide layer left on the top surface of the sensitive area as an intermediate layer for the solar-blind filter stack deposition. The response starts to cut off at approximately 375 nm, corresponding to the bandgap of 4H-SiC. The fabricated SiC APDs did not show a measurable response to visible light at wavelengths greater than 400 nm. The long-wavelength cutoff is not sharp due to the indirect bandgap nature of SiC and thus an additional solar-blind optical filter was required to suppress responsivity in the 300 nm - 400 nm wavelength range in order to achieve a high solar photon rejection ratio in the near-UV range.

Dark current density curves of a typical SiC APD 8x8 array are shown in Figure 9. It was possible to distinguish three characteristic groups (A, B and C) of the dark current curves for each array. Group A consists of APD devices with the lowest dark currents and very sharp avalanche breakdowns. Group B consists of APD devices with moderate leakage currents and less sharp avalanche breakdowns, while Group C consists of APD devices with high leakage currents and soft breakdowns. Note, that a value of a breakdown voltage for all devices for this array was 186±3 V at a current density of 10^{-4} A/cm^2. A histogram distribution of current densities measured at 95% of U_{BD} is shown in Figure 10. One may see that the number of devices from Group A with a current density of ~10nA/cm^2 was 28 or 43 % per array of 64 devices, while numbers of devices from Groups B and C were 28 (43%) and 8 (14%), respectively.

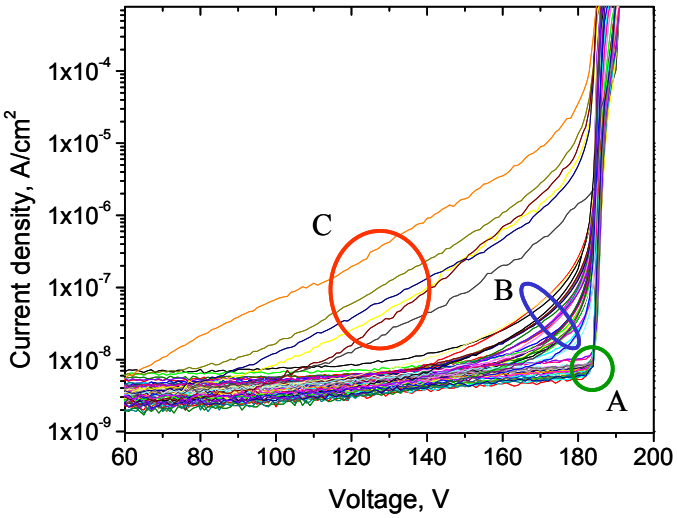

Figure 9: Dark current density curves of typical SiC APD 8x8 array.

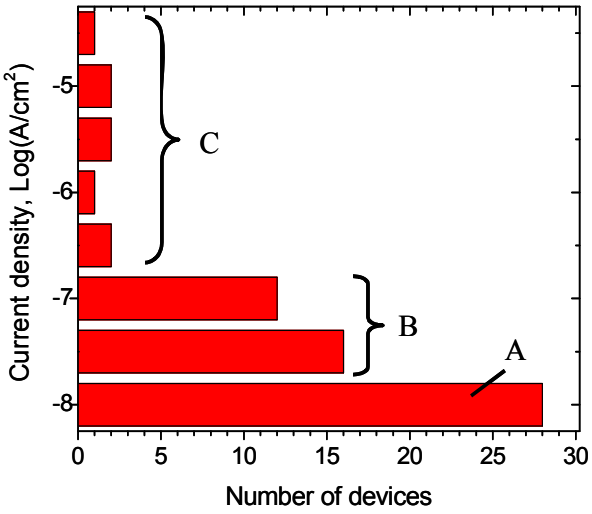

Figure 10: *Distribution of current densities at 95% of a breakdown voltage in individual APDs in typical 8x8 array*

Using the Electron Beam Induced Current (EBIC) technique it has been found that such a variation in leakage currents is associated with different numbers of dislocations in SiC substrates that contained an individual APD device in the array. Moreover, the devices from Group A (with the lowest leakage currents) were found to be defect-free devices.

3.4. Single Photon Detection Efficiency

The SPDE is an important characteristic of the avalanche photodiode and can be defined as the product of the quantum efficiency and the avalanche probability when operated at reverse biases above the breakdown voltage. Two passive quenching methods were used to measure single photon detection efficiency of devices without solar-blind filter. The first "quasi-Geiger" method was utilizing simple asynchronous passive resistive quenching and the second method was using passive gated quenching.

Figure 11 shows the schematic of the measurement setup. A 266 nm laser beam focused within the device with an average of 0.3 photons during a 500-ps pulse and an 8.3 kHz repetition rate was used in both methods to illuminate the device. The breakdown voltage was measured to be around 194 V and the bias voltage for the "quasi-Geiger" mode measurements was swept between 193 V and 200 V. The SPDE and dark count rate were measured for the same bias to obtain the curve shown in Figure 12.

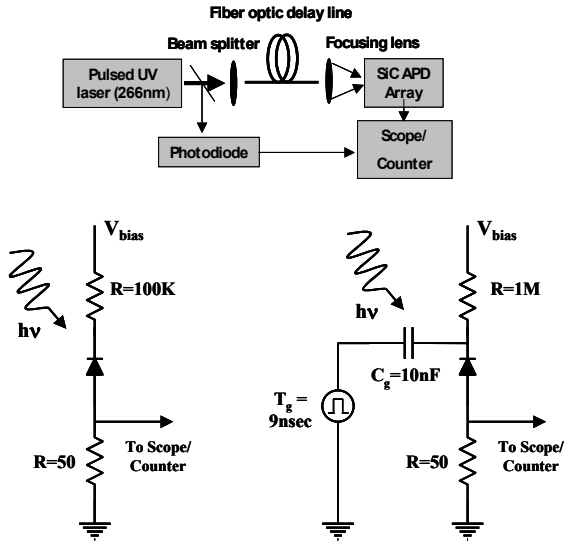

Figure 11: *Block diagram and schematics of the photon detection efficiency measurements in the Geiger mode: asynchronous passive quenching – left, passive gated quenching – right*

For gated passive quenching Geiger mode measurements, the dc bias voltage was set fixed at 190 V, or 4 V below the breakdown voltage. The excess ac-coupled voltage above the dc voltage was applied during a 9-ns gate pulse. The arrival of the photon was synchronized with the gate pulse. The avalanche pulses were discriminated and counted within a 1 nanosecond window. The excess voltage was scanned in the range from 5 to 30 V. Figure 13 shows the SPDE versus the dark count probability measured for the

same over-bias. Three tested devices from different group (A, B and C) demonstrated different dark count rates and dark count probabilities. The difference in the dark characteristics can be explained by the presence of defects. In general, passive gated quenching demonstrated higher gains and better single photon detection efficiency, but ungated linear mode measurements have also demonstrated promising results. The simplicity of asynchronous passive quenching is one of the attractive advantages, although the detection efficiency is greatly reduced in devices with large number of dark counts. In such devices, the interference from dark counts affects sensitivity, suggesting that the passive gated quenching or asynchronous active quenching is a better quenching scheme to limit the amount of charge flown through the APD. Another complication arising from the operation of 4H-SiC APDs without fast quenching is the amount of after pulses initiated by the residual charge.

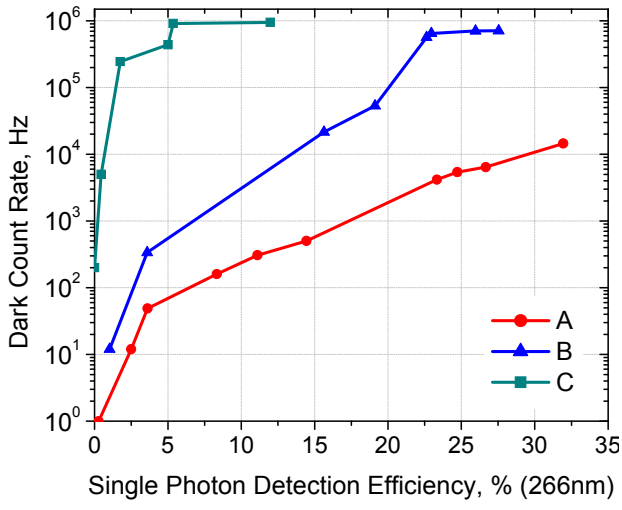

Figure 12: *Asynchronous resistive quenching dark count rate versus single photon detection efficiency at 266nm*

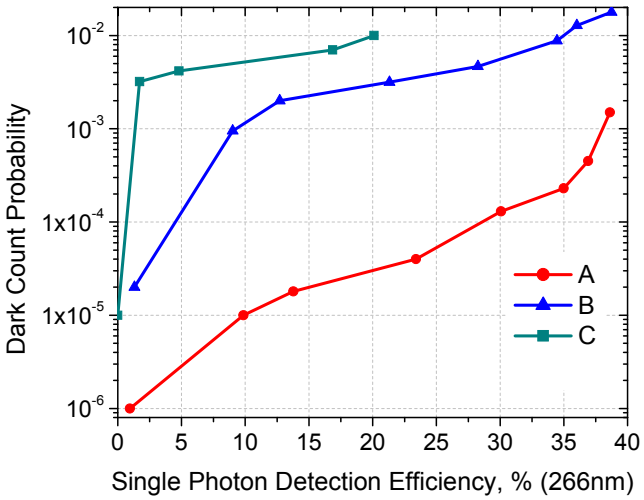

Figure 13: *Passive gated quenching Geiger mode dark count probability versus single photon detection efficiency at 266nm.*

Separate absorption and multiplication 4H-SiC APDs have demonstrated 47% quantum efficiency at 280 nm wavelength. Single photon detection efficiencies of 32% and 37% were achieved at 266nm wavelength for passive quenching mode and gated Geiger-mode respectively. A dark count rate 10 kHz and a corresponding dark count probability of 10^{-4} were recorded with the best device at a reverse bias providing the single photon detection efficiency more than 30%.

3.5. Actively-Quenched Geiger-Mode Operation with Time-of-Arrival Tagging

Active quenching can provide the fastest reset times, and therefore the lowest blocking loss and highest achievable operational bandwidth for an array of GM-APDs. The active quenching circuitry for each APD can be combined with a precision clock reference and detection logic to enable each photon detection event to be time-tagged with a precision substantially better than 1 nanosecond. The combined quenching, detection, and time-tagging circuitry, termed a read-out IC (ROIC), can be bump-bonded to an appropriately designed GM-APD array to form a compact integrated circuit for use in time-resolved photon-counting applications such as ladar[15]. In concert with the development of SiC GM-APD arrays by GE, MIT Lincoln Laboratory is fabricating a prototype 4x4 ROIC that will be wirebonded to a 4x4 APD array to demonstrate high-speed UV-C single photon detection and time tagging. A demonstration of the 4x4 prototype, scheduled for May of 2009, will provide quantitative performance metrics to guide the design of larger size arrays bump-bonded directly to a ROIC.

3.6. Solar-Blind filter

Figure 14 shows the external quantum efficiencies of devices with and without near-UV blocking filters measured in the wavelengths range from 200 to 1000 nm at a reverse bias of 50 V. Devices with external and integrated solar blind filters showed rejection ratio of at least 10^6 for visible photons, but the rejection ratio of near-UV photons was slightly

lower than expected in devices with integrated filter. The external quantum efficiency of filtered devices was 37% at 280 nm, due to the 20% transmission loss of the solar blind filter. Transmission spectra of the optical filter deposited on sapphire substrate for different angles of incident light is shown in Figure 15. These measurements demonstrate that wavelength cut-offs on both sides of the by-pass filter shift into deep-UV part of the spectrum with increasing angle of incident. Moreover, the transmission peak is down 8% at an incidence angle of 30 deg, and 25% at an angle of 45 deg.

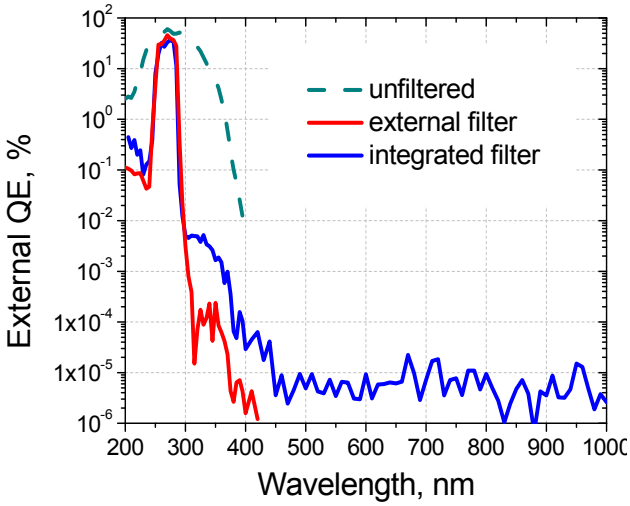

Figure 14: Measured external quantum efficiency of 4H-SiC SAM APDs with no filter, integrated filter, and external filter

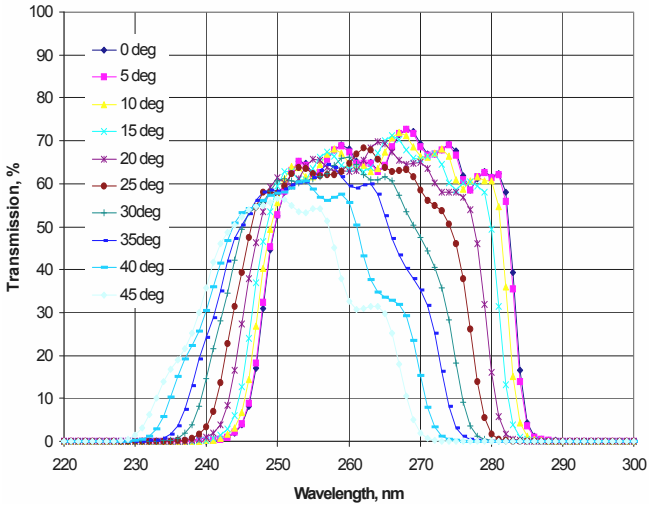

Figure 15: *Transmission spectra of the optical filter deposited on sapphire substrate for different angles of incident light.*

3.7. Performance comparison

SiC GM-APD arrays are an emerging technology, and arrays produced to date have not yet been integrated with high-speed ROICs. Nonetheless, it is instructive to compare the expected performance of hybridized SiC GM-APDs with the performance achievable using existing COTS detectors, in particular the CsTe CPM and the passively-quenched Si GM-APD arrays discussed in Section 2.2. Table 3 compares these detectors on the basis of the performance metrics defined in Section 2.1.

Table 3: *Performance comparison of SiC APD array goals with CsTe CPM and Si MPPC arrays*

Detection Performance	**CPM CsTe Detector**	**MPPC Array Detector**		**SiC GM-APD Active-Quenching**
Parameter	**MP-1921**	**50μm**	**25μm**	**DUVAP Goals**
Single detector				
– QE or SPDE (270nm)	8 %	32 %	26 %	40 %
– QE or SPDE (400nm)	.01 %	86 %	81 %	.01 %
– Area (A)	192 mm^2	.002 mm^2	.0005 mm^2	~.008 mm^2
– DCR per device	.005 kHz	0.75 kHz	0.375 kHz	5-10 kHz
– Bandwidth (BW)	5 MHz	25+ MHz	50+ MHz	100 MHz
Detector array				
– Number of detectors	1	20x20	40x40	16x16
– Fill factor	100 %	61.5 %	30.8 %	50%
– Active area	192 mm^2	.615 mm^2	.31 mm^2	3-8 mm^2
– Recovery time	~ 100 ns	35 ns	20 ns	10 ns
– DCR per array	.005 kHz	400 kHz	300 kHz	1280 - 2560 kHz
– Normalized DCR	.026 kHz/mm^2	650 kHz/mm^2	970 kHz/mm^2	320-425 kHz/mm^2

4. APPLICATIONS

Successful development of wide-bandgap, solar-blind, actively-quenched GM-APD arrays will not entirely replace PMTs, but can provide enhanced performance in some applications, and will enable new applications that were previously not feasible. In this section, a few examples of applications enhanced or enabled by deep-UV photon-counting GM-APD arrays are presented.

4.1. Bio-aerosol detection

Bio-aerosol detection is an important first step in both military and civilian biodefense strategies. An unrealized goal has been the development of a small, low-cost, highly reliable bio-aerosol detection sensor that could be installed throughout buildings and other public venues much like smoke alarms. To realize this goal, a key component is a low-cost, low-power photon-counting detector capable of operating in the UV-C and UV-B bands, since UV-C pulses are used to stimulate the fluorescence of individual particles in the sensor, and photon counting is used to measure the elastic scattering as well as the induced fluorescence signatures characteristic of biological particles[16]. In terms of requirements, the biosensor application allows for baffling of the measurement volume to eliminate ambient light, so intrinsic rejection of visible light is not important. For bio-aerosol detection, an active area of $1mm^2$ or larger and a PDE of 20% or better are desired. Dark count rates of less than 10 kHz are required, since the signal is weak and the observation time is long.

The basic geometry employed in bio-aerosol detectors is illustrated in Figure 16, where one or more PMTs are typically employed to perform the necessary photon counting. In the system of Figure 16, particles flow through the detection volume in a stream of air while a pulsed UV LED is used to probe the passing particles to determine if they fluoresce, indicating the possible presence of biological compounds.

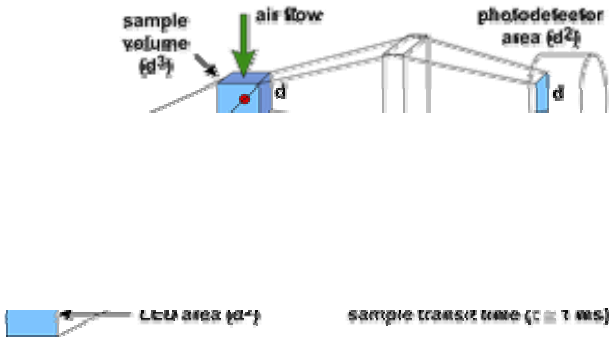

Figure 16: *Schematic of a compact bio-aerosol detector*

Replacing the PMT with an addressable array of GM-APDs will enhance system performance by providing a mechanism to track the moving particles along the direction of air flow, performing time-delay integration to improve the signal to noise ratio prior to detection. In this case, the individual detectors in the array should exhibit dark counts of less than 5kHz. Optical design of the system for tracking will benefit from a detector implementation that is compatible with microlens hybridization.

4.2. Micro Flash Ladar for navigation

The extinction length of UV-C in the atmosphere is on the order of 1 km, which precludes long-range ladar applications. However, for short-range navigation by unmanned ground or air vehicles, a UV-C ladar system has the advantage of benign backgrounds and few anthropogenic sources of interference to confuse or blind the photon-counting detector.

When employed for flash ladar ranging, all of the APDs in the array are reset at the start of the range window and each APD (pixel) has a unique field of view that overlaps with adjacent pixel fields of view, analgous to a digital camera. Unlike a digital camera, however, a pixel will only record the first (usually the closest) range return within its field of view since once the APD fires, the reset time is a significant fraction of the range window. However, multiple pulses and image frames can be collected and averaged to reduce false alarms from dark counts and improve the probability of detecting returns from porous surfaces at multiple ranges. Since there are few anthropogenic sources and no solar background to contend with, each pixel can operate over a large solid angle (using low f/# imaging optics) to maximize the detected irradiance, constrained only by the angular resolution required for the navigation system at the ranges of interest. The beamwidth of the flash illuminator must be commensurate with the aggregate field of view of the detector array as indicated in Figure 17.

A micro ladar for navigation should provide range resolution of 30cm or better for object location and avoidance, corresponding to range time bins (photon counting intervals) of 1-2ns or less. For daytime operation, near-UV and visible light leakage must be low enough to ensure that the probability of an APD triggering on background is low for the duration of the range window. A 500m range window corresponds to a range delay time of 3.3μs, implying the background leakage counts for a given GM-APD should be 300 kHz or less. This near-UV/visible blocking performance can be realized if the intrinsic solar rejection of the device plus blocking filter achieves at least 50dB of suppression over the near-UV and visible bands.

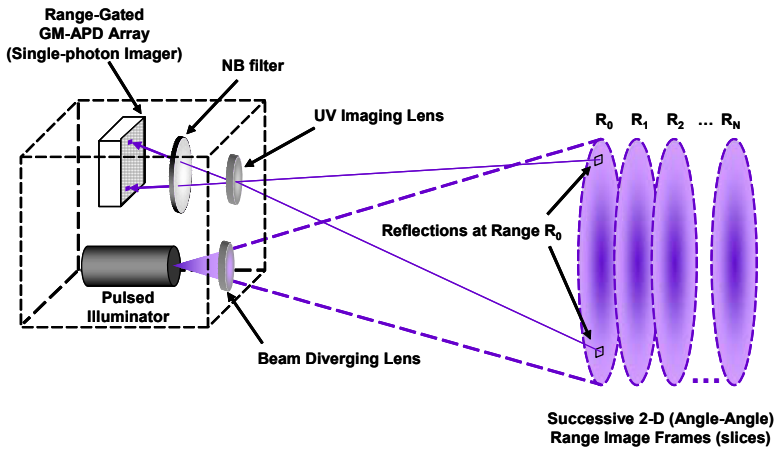

Figure 17: *Schematic of a flash ladar imaging system*

For the same reason, the aggregate dark count rate of the APD array must be <300 kHz, relative to the duration of the range window. The use of a microlens array also improves collection efficiency and implies that the APD detector areas can be small, on the order of 10-20 μm, which helps to reduce the intrinsic dark count rate.

4.2.1. Deep-UV Imaging

A variety of reflection- and scatter-based UV imaging applications exist, including imaging of scratches and imperfections on surfaces, detecting high-voltage corona discharges, visualizing sun-induced skin damage and bruises, detecting trace evidence and organic contamination on surfaces, and imaging cells and biological organisms. The strong absorption of deep-UV by most transparent materials is used to advantage here, since by limiting the interaction depth, it significantly reduces image clutter from bulk scattering within the material. In most of these applications, the introduction of a photon-counting detector can improve the system performance either by reducing the required levels of illumination, or by enabling the detection of weaker reflections.

The imaging application envisioned here is based on the previously described flash ladar concept, but requires larger GM-APD arrays than currently exist, and application of a different processing methodology to the time-tagged single photon detections. The concept is intended to augment night vision by pairing a UV-C flash illuminator with a fast-frame photon-counting SiC GM-APD array to create a single-photon imager. Although this concept could be developed at longer wavelengths, a long-wave system would be more easily detectable by conventional imaging systems at standoff ranges, whereas a UV-C illuminator is inherently more covert. Furthermore a UV-C imaging system would not be susceptible to blinding through inadvertent or intentional illumination by a visible or IR

(a) (b)

Figure 18: *Canadian arctic camouflage and toboggan (a) Visible image (b) near-UV image (300-400nm, peak sensitivity 370nm) rendering camouflage ineffective (courtesy Dr. David Lavigne)*

source. There is also evidence that a UV-C imaging system may help to discriminate between natural and man-made objects in a scene. Figure18 illustrates an example of detecting white arctic camouflage by virtue of the fabric's strong absorption of near-UV light. Similar differences in reflectance and absorption can be exploited in the UV-C band.

In the enhanced night-vision concept, a UV-C flash illuminator and 2-D GM-APD array function as a 3-D imaging ladar, forming single-photon images at successive ranges by synchronously range-gating the APD array with the illumination pulse. Multiple single-photon image frames can be collected at each range over a period of time in order to form grey-scale intensity images of the scene. Such a system can be operated in various modes, depending upon the gating of the APD array. To form conventional images at a 60Hz frame rate, single-photon image frames would be collected at the rate of ~5000 every $1/60^{th}$ second and averaged to form a grey scale image. The number of dark counts over the time interval of 1/60 = 16.6ms must be small relative to the signal levels from the illumination pulse. A nominal threshold for dark count performance in the APD array would be on the order of 100 dark counts per 60 Hz frame or a dark count rate of less than 6kHz.

A second mode of operation for the active UV imager is to present the angle-angle-range 3-D point cloud collected over multiple frames to the user in a manner that allows the user to manipulate the point cloud to search for objects and information in the scene. In Figure 19, a sample point-cloud image collected with a 30mW 532nm ladar is shown[17].

Additional information on conventional UV imaging and a comparison with photomultiplier technology is available in an article by Lavigne et al.[18]

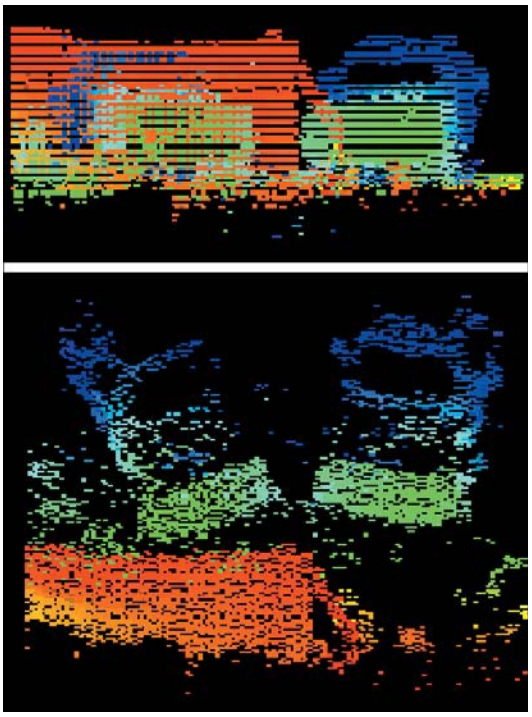

Figure 19: *Two different views of a 3-D ladar point cloud consisting of two vehicles, one parked behind a camouflage net. Range is color-coded with orange the near range and blue the far range.*

4.3. Harsh-Environment UV and Gamma Detectors

A class of applications that will benefit from advancements in SiC detector technology are those associated with harsh environments such as gas turbine flame monitoring, down hole gamma sensors, and instrumentation where high temperature tolerance and ruggedness is key. Silicon detectors and PMTs typically need additional cooling to survive and operate in harsh environments. The large bandgap provides unique advantages for long-term operation of 4H-SiC photodiodes and avalanche photodiodes at high temperatures above 200ºC.

SiC-based UV detectors (coupled with a scintillator crystal) are an especially promising detector alternative to aid in oil exploration in remote, harder to reach locations around the world. The average depth of exploratory wells has grown over 1,000 feet over the past 25 years, a trend which is expected to continue. While each well location may have a

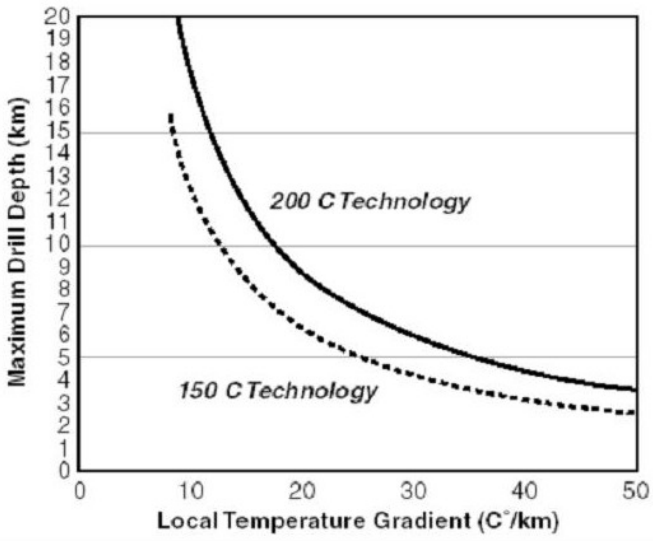

Figure 20: *An estimate of the temperature incurred while drilling versus local temperature gradient*

different temperature dependency as a function of depth, a general rule of thumb may be applied in which the temperature increases with depth roughly between 10 and 50 ºC/1,000 meters. In Figure 20, a comparison of maximum drill depth is shown between two different technologies with capability to operate at 150 and 200 ºC. An operating temperature increase of just 50 ºC would enable substantially deeper drilling at many sites.

SUMMARY AND CONCLUSIONS

To date, applications requiring photon counting in the deep-UV have primarily relied upon solar-blind PMTs to perform the detection function. Benefits of PMT detectors include large active areas and low dark-count rates. Near the edge of the solar-blind region, UV-enhanced silicon GM-APD detectors can be employed to achieve higher bandwidths and enable array configurations. However, providing adequate solar blocking to enable the use of silicon APDs in outdoor applications is challenging and costly. Furthermore, individually addressable and resettable silicon GM-APD arrays are not available commercially, limiting the range of applications for photon-counting.

SiC GM-APD arrays will provide higher SPDE performance in the deep-UV than existing PMT or silicon arrays and better rejection of solar background. When combined with near-UV blocking filters, the SiC GM-APD arrays described in this paper will enable new classes of applications by providing low-cost, low-power, individually addressable pixel arrays with high SPDE and good solar rejection. Several applications for deep-UV photon counting have been discussed at the conceptual level to illustrate that required dark count rates and array size are application independent. For example, small size arrays with high dark counts can be employed successfully in flash ladar systems for navigation. As GM-APD devices mature, larger arrays with lower dark counts will enable new types of applications including bio-aerosol detection and flash imaging.

ACKNOWLEDGEMENTS

The authors dedicate this paper to the memory of Dr. Henryk Temkin of DARPA, for his vision in creating the DUVAP program and his lifelong dedication to the advancement of science and education.

This work was sponsored by DARPA under contract FA8721-05-C-0002. Opinions, interpretations, conclusions and recommendations are those of the authors, and not necessarily endorsed by the United States Government.

REFERENCES

[1] http://optoelectronics.perkinelmer.com/content/datasheets/dts_cpmmpseriesb.pdf (2009)

[2] http://www.sensl.com/pdfs/Datasheets/SPMMini_Datasheet.pdf (2009)

[3] http://jp.hamamatsu.com/products/sensor-ssd/4010/index_en.html (2009)

[4] Isoshima, T., Isojima, Y., Hakomori, K., Kikuchi, K., Nagai, K., and Nakagawa, H., "Ultrahigh sensitivity single-photon detector using a Si avalanche photodiode for the measurement of ultra weak biochemiluminescence.," Rev. Sci. Instrum., vol.66, no. 4, 2922–2926 (1995).

[5] Limb, J.B., Yoo, D., Zhang, Y., Ryou, J. H., Schen, S.C., Dupuis, R.D., "GaN ultraviolet avalanche photodiodes grown on 6H-SiC substrates with Si N passivation," Electronic Letters, vol. 44, no. 4, 313-314 (2008).

[6] Verghese, S., McIntosh, K.A., Molnar, R.J., Mahoney, L.J., Agrawal, R.L., Geis, M.W., Molvar, K.M., Duerr, E.K., and Mengalis, I., "GaN avalanche photodiodes operating in linear-gain mode and Geiger mode," IEEE Trans. Electron Devices, vol. 48, 502–511 (2001).

[7] Jiang, H., Egawa, T., "Low-Dark-Current High-Performance AlGaN Solar-Blind p-i-n Photodiodes," Japanese Journal of Applied Physics, Part 1: Regular Papers and Short Notes and Review Papers, vol. 47, no. 3, 1541-1543 (2008).

[8] Xin, X., Yan, F., Sun, X., Alexandrove, P., Stahle, C.M., Hu, J., Matsumara, M., Li, X., Weiner, M., and Zhao, H.J., "Demonstration of 4H-SiC UV single photon counting avalanche photodiode," Electron. Letters, vol. 41, no. 4, 212-214 (2005).

[9] Guo, X., Beck, A.L., Huang, Z., Duan, N., Campbell, J.C., Emerson, D., Sumarekis, J.J., "Performance of low-dark-current 4H-SiC avalanche photodiodes with thin multiplication layer," IEEE Trans. Electron Devices, vol. 53, no. 9, 2259-2265 (2006).

[10] Jun H., Xiaobin, X., Xueqing, L., Zhao, J., VanMil, B., Lew., K., Myers-Ward, R., Eddy, C., Gaskill, D., "4H-SiC Visible-Blind Single-Photon Avalanche Diode for Ultraviolet Detection at 280 and 350 nm," IEEE Transactions on Electron Devices, v 55, n 8, 1977-83 (2008).

[11] Zhu, H., Chen, X., Cai, J., Wu, Z., "4H–SiC ultraviolet avalanche photodetectors with low breakdown voltage and high gain," Solid-State Electronics, vol. 53, no. 1, 7-10 (2009).

[12] Bai, X., Liu, H., McIntosh, D., Campbell, J., "High-performance SiC avalanche photodiode for single ultraviolet photon detection," Proceedings of SPIE - The International Society for Optical Engineering, v 7055, Infrared Systems and Photoelectronic Technology III, 70550Q (2008).

[13] Bai, X., Gou, X., McIntosh, D.C., Liu, H., Campbell, J.C., "High Detection Sensitivity of Ultraviolet 4H-SiC Avalanche Photodiodes," IEEE J. Quantum El., Dec., vol. 43, no. 12, 1159-1162 (2007).

[14] Barr Associates, Inc. Westford, MA 01886 USA.

[15] Verghese, S., et al, "Arrays of InP-based Avalanche Photodiodes for Photon Counting," IEEE Journal of Selected Topics in Quantum Electronics, vol 13, no. 4, 867-883 (2007).

[16] Jeys, T., Herzog, W., Hybl, J., Czerwinski, R., Sanchez, A., "Advanced Trigger Development," Lincoln Laboratory Journal, vol 17, no. 1, 29-62 (2007).

[17] Albota, M. A., et al., "Three-Dimensional Imaging Laser Radars with Geiger-Mode Avalanche Photodiode Arrays," Lincoln Laboratory Journal, vol 13, no. 2, 351-370 (2002).

[18] Lavigne, C., Roblin, A., Langlois, S., "Solar-blind UV imaging photon detector with automatic gain control," Measurement Science and Technology, No. 13, 713-719 (2002).